More Frequent Spaceborne Sampling of X_{CO2} Improves Detectability of Carbon Cycle Seasonal Transitions in Arctic-Boreal Ecosystems

Nicholas C Parazoo[1], Gretchen Keppel-Aleks[2], Stanley Sander[1], Brendan Byrne[1], Vijay Natraj[1], Ming Luo[1], Jean-Francois Blavier[1], Len Dorsky[1], Ray Nassar[3]

[1]Jet Propulsion Laboratory, California Institute of Technology

[2]University of Michigan, Climate and Space Sciences and Engineering

[3]Environment and Climate Change Canada

Corresponding author: Nicholas Parazoo (nicholas.c.parazoo@jpl.nasa.gov)

Key Points:

- The Arctic Fourier Transform Spectrometer Investigation (AURORA) mission concept addresses GHG sampling limitations in the Arctic
- AURORA uses a highly elliptical orbit (HEO) to increase repeat frequency, and a panchromatic iFTS for wide spectral range (0.7–15.4 μm)
- Increased sampling frequency in the SWIR improves detection of spatial gradients in cold season efflux in the Arctic relative to OCO-2

Abstract

Surface, aircraft, and satellite measurements indicate pervasive cold season CO_2 emissions across Arctic regions, consistent with a hyperactive biosphere and increased metabolism in plants and soils. A key remaining question is whether cold season sources will become large enough to permanently shift the Arctic into a net carbon source. Polar orbiting GHG satellites provide robust estimation of regional carbon budgets but lack sufficient spatial coverage and repeat frequency to track sink-to-source transitions in the early cold season. Mission concepts such as the Arctic Observing Mission (AOM) advocate for flying imaging spectrometers in highly elliptical orbits (HEO) over the Arctic to address sampling limitations. We perform retrieval and flux inversion simulation experiments using the AURORA mission concept, leveraging a Panchromatic imaging Fourier Transform Spectrometer (PanFTS) in HEO. AURORA simulations demonstrate the benefits of increased CO_2 sampling for detecting spatial gradients in cold season efflux and improved monitoring of rapid Arctic change.

1 Introduction

Anthropogenic warming is occurring 3-4 times as fast in the Arctic compared to the global mean, potentially unlocking climate feedbacks with global implications (Rantanen et al., 2022). The changing Arctic carbon balance is a critical global uncertainty to future climate warming, and processes that control this balance are already responding to warming (Natali et al 2019; Bruhwiler et al 2021). Climate change has been shown both to increase photosynthetic uptake of CO_2, and to accelerate emission of CO_2 back into the atmosphere (Jeong et al 2018). The balance of these competing processes is an important determinant of whether the Arctic remains a net sink for CO_2, — current sink magnitude estimated as 850 TgC (Watts et al., 2023) — or transitions to a net source.

Growing evidence from Arctic and boreal site-level flux (Natali et al 2019; Watts et al 2021), and tower and satellite CO_2 concentration measurements (Liu et al 2022; Byrne et al 2022), indicate pervasive CO_2 release during the early cold season (Sep–Dec) across the pan-Arctic. These emissions are linked to warmer soils and increasingly labile carbon and have significant impacts on annual carbon budgets. The spatial extent of these emissions is well characterized at local scale (1–2 km) from flux towers, and at sub-continental scale (> 1000 km) from tower and satellite observations. However, the interactions between climate change and carbon storage vary regionally, at scales between the current generation of flux tower networks and satellite observing capabilities, due to season, ecosystem type, and permafrost condition. Aircraft campaigns can help fill these gaps (e.g., Parazoo et al., 2016; Commane et al., 2017; Schiferl et al., 2022) but are impractical for continuous pan-Arctic coverage, leaving key observational gaps in remote regions such as Siberia, where significant carbon losses are already occurring at regional scale (Liu et al 2022), and which are likely to become amplified in the next decades as ancient carbon reserves buried deep in the soil thaw and decompose. Moreover, hotspots of abrupt and irreversible carbon loss may not be observed by spatially and temporally sparse field campaigns, and infrequent satellite measurements.

There remains a knowledge gap in existing observing systems owing to (a) spatially sparse field measurements, (b) spatially and temporally limited and sporadic airborne campaigns, and (c) low repeat frequency (1–2 times per month) of existing satellite CO_2 data. While satellites offer the best opportunity to provide consistent pan-Arctic coverage, existing measurements are too infrequent to detect abrupt emissions or resolve vegetation gradients, and coverage falls off steeply outside summer as northern high latitude (NHL; latitudes > 45°N) data coverage and quality succumb to clouds, snow, and polar darkness. New mission concepts focused on frequent and continuous coverage in space and time over multiple consecutive years are needed to detect emissions and provide new information relevant to improving process understanding.

Here, we examine one possible observing strategy to help address the above-mentioned sampling limitations and provide more detailed understanding of pan-Arctic carbon cycling (Figure 1). This strategy leverages key innovations in instrument design and observing platform. First, we use a Panchromatic imaging Fourier Transform Spectrometer (PanFTS) that utilizes high-speed digital focal plane arrays to record shortwave infrared (SWIR) spectra from each pixel of a 2-D array. Second, data is obtained from a unique 12-hour highly elliptical orbit (HEO) that observes both North American and Eurasian high latitude regions for up to 8 consecutive hours each. This approach stems from the Arctic Observing Mission (AOM, Nassar et al., 2023) (formerly AIM-North, Nassar et al., 2019), which will carry an imaging spectrometer for making SWIR measurements of CO_2, CH_4, and CO in HEO. This idea developed out of an earlier HEO FTS concept (Nassar et al., 2014). Some of the key advantages of employing imaging spectrometers such as PanFTS in HEO include the following:

1. SWIR observations provide near-surface sensitivity,
2. Collocation of three carbon species (CO_2, CO, CH_4) supports chemical-based process attribution,
3. Large focal plane array (640 × 480) enables mapping of spatial gradients,
4. Frequent repeat cycle (90 minutes) facilitates observations of fast-evolving events (e.g., fires)
5. Sub-daily year-round observations help to more accurately determine (1) seasonal controls on uptake versus release of modern carbon, using CO_2 column observations, (2) spatial and temporal extent of carbon emissions in response to episodic warming, and (3) carbon balance of fire and processes that affect recovery after burn.

As demonstrated by Natraj et al. (2023), PanFTS uses a wide spectral range (1–15.4 μm) encompassing both SWIR and thermal infrared (TIR) bands, which can help separate near-surface and mid-tropospheric variability and enable vertical profiling of water vapor, temperature, and greenhouse gases (GHGs). This capability has potential to further augment carbon cycle science in the Arctic through improved sampling in polar winter and over ocean, and better characterization of background influences (e.g., Parazoo et al., 2016), but is beyond the scope of this paper. Here, we focus on using PanFTS SWIR bands to retrieve CO_2 concentration and flux using end-to-end Observation System Simulation Experiments (OSSEs) to show potential gains in tracking (1) seasonal change across the transition season and early cold season, and (2) grid scale fluxes. To gauge improvement over the Program of Record (PoR), we compare PanFTS-based flux retrievals to those from OCO-2, the latter providing infrequent (16-day repeat) but widespread spatial coverage. Given the challenges of implementing a regional mission focusing for example on NHLs in a global inversion, we design OSSEs starting with OCO-2, and then combining with PanFTS in a HEO configuration similar to AOM. We describe the HEO orbit, PanFTS retrievals, and CO_2 flux inversion experiments in more detail in Section 2, present first results for PanFTS retrievals and flux inversions across the pan-Arctic in Section 3, and finally discuss the implications of these results in Section 4.

2 Materials and Methods

We designed an end-to-end OSSE to determine the added benefit of PanFTS CO_2 retrievals with respect to OCO-2 based inferences of grid- and regional- scale CO_2 flux across NHLs. Our approach is based on existing models for (1) retrieval of column integrated CO_2 mixing ratio (XCO_2) in SWIR bands using the PanFTS instrument configuration, and (2) inversion of XCO_2 for obtaining grid scale CO_2 flux. These models are summarized below. We henceforth refer to the PanFTS HEO observing strategy as the Arctic Fourier Transform Spectrometer Investigation, or AURORA.

2.1 Molniya Orbit

For AURORA, we assume a single PanFTS flying in HEO, observing over land from 30–90°N multiple times per day (Figure 1). The slow movement of the satellite at apogee is well suited for the long stare time requirements of imaging spectroscopy. PanFTS requires 6 minutes of integration time per field of view (FOV) for day-time scans in the SWIR. This translates to 84 minutes to scan over the field of regard (FOR) at the summer solstice. The 12-hour HEO orbit, with an apogee altitude of 39700 km, inclination of 63.4°, and eccentricity of 0.722, could in principle provide 8 hours of total view time of the sunlit hemisphere, providing quasi-stationary sub-daily coverage of the pan-Arctic. However, we exclude samples beyond 2 hours of apogee due to significant instrument drift and potential detrimental impacts to coverage, ground sampling distance, and retrieval calculations. We therefore assume two revisits per orbit within 90 minutes of Apogee, enabling two full summer visits per orbit. We furthermore assume the Apogee is centered over boreal North America (63.4°N, 85°W) for the first orbit and over boreal Eurasia (63.4°N, 95°E) for the second orbit, to minimize off-nadir land views.

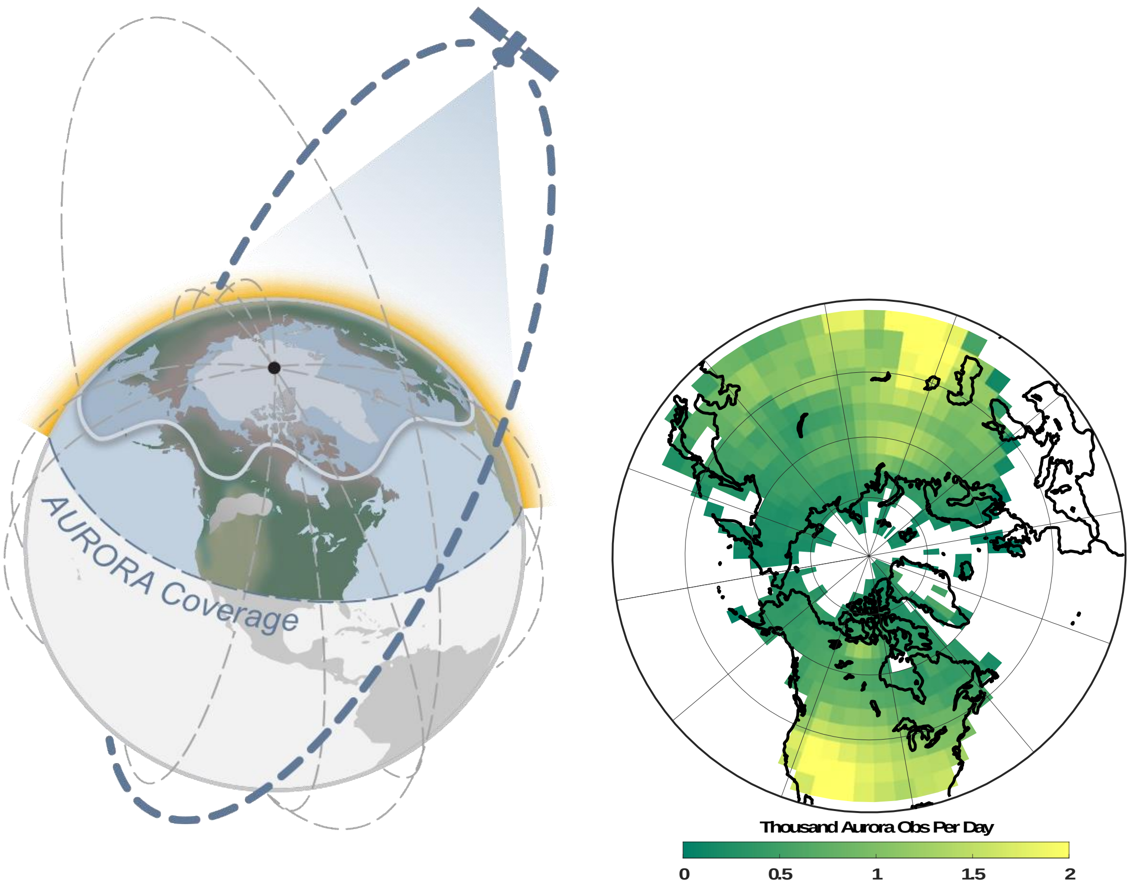

Figure 1: AURORA Schematic + Map of Sampling Coverage. (left) AURORA is comprised of the Panchromatic Fourier Transform Spectrometer (PanFTS) deployed in a highly elliptical orbit centered on North America and Siberia, providing sub-daily mapping of key greenhouse gases (CO_2, CO, CH_4) over pan-Arctic oceanic and land regions. (right) AURORA cloud-free sampling per day, averaged over one year. AURORA provides sampling rates on the order of 1000 samples per month per 5° × 5° on an annual basis, representing a period of widespread CO_2 efflux across the pan-Arctic (see Fig S3 for monthly sampling rates). AURORA aims to reduce uncertainty in the magnitude and distribution of grid-scale fluxes during this critical transition period.

2.2 CO_2 Retrieval from PanFTS Observations

We examine atmospheric profiles spanning multiple locations (one in central Alaska and one in eastern Canada), times of day (afternoon and evening), seasons (spring and fall equinox, summer and winter solstice), land cover types (forest and snow), and solar zenith angles (SZA) in North America (parameters summarized in Table S1).

We use the two-stream-exact-single-scattering (2S-ESS) radiative transfer (RT) model (Spurr and Natraj, 2011; Natraj et al., 2023) to generate monochromatic radiances at the top of the atmosphere for the atmospheric profiles and surface conditions in Alaska and Canada over the entire PanFTS spectral range. The model and experiments follow the same basic setup described by Natraj et al (2022), which provides a scoping study for retrieving multiple GHGs (CO_2, CH_4, and CO) over temperate North America.

The PanFTS instrument model is similar in design to the GEO-IR Sounder (Natraj et al, 2022), which allows exploration of the instrument trade space and its effect on retrieved atmospheric composition. It reads synthetic data from the RT model, convolves synthetic spectra and Jacobians with the instrument line shape (ILS), converts spectra into an interferogram, and computes photon noise and signal to noise ratio. To optimize the tradeoff between frequent sub-daily sampling and cloud free pixels in HEO, we assume a ground sampling distance (GSD) of 4 km from the 39700 km apogee. A 4 km ground pixel subtends an angle of 58.7 μrad and for a Focal Plane Array (FPA) of 540 × 540 pixels; the overall FOV is 60 mrad. The PanFTS optics uses a triple-band optical filter to narrow SWIR interferometer output to the following spectral regions for CO_2: (1) 2.000–2.433 μm, covering the strong CO_2 band near 2.1 μm, (2) 1.565–1.695 μm, covering the weak CO_2 band near 1.61 um, and (3) 1.233–1.302 μm, covering the 1.27 μm oxygen band needed to measure the light path. The time per interferogram point is 10 ms for SWIR and 2.5 msec for the O_2 band.

We employ the widely used optimal estimation approach (Rodgers, 2000) and perform linear retrievals (e.g., Kulawik et al., 2006) of CO_2 from simulated radiances based on the instrument model. The a priori constraint vectors for temperature (TATM), water vapor (QV), and CO_2 are obtained at the time and location of the scenarios in Table S1. TATM is taken from Tropospheric Emission Spectrometer (TES) retrievals (https://tes.jpl.nasa.gov/tes/data/products/level-2), H_2O from MERRA-2 reanalysis (https://gmao.gsfc.nasa.gov/reanalysis/MERRA-2/), and CO_2 from the GEOS-Chem tracer transport model (e.g., Byrne et al., 2023). We prescribe TATM from TES, rather than MERRA-2, to provide a more realistic estimate of the tropopause and stratospheric profile. CO_2 data are constrained using posterior CO_2 fluxes derived from Greenhouse gases Observing SATellite (GOSAT) CO_2 observations in the CMS-Flux inversion system (Byrne et al., 2023). The representative atmospheric profiles for each species show expected vertical and seasonal behavior for the Arctic region (Figure S1). A priori constraint matrices are constructed using the method described in Kulawik et al (2006).

2.3 CO_2 Flux Inversion OSSE

PanFTS retrieval cases are propagated to full year-round pan-Arctic sampling based on time of day and year, land cover, solar zenith angle (SZA), and cloud presence. Land cover is identified using the MERRA-2 snow fraction (snow fraction >= 0.2 indicates snow, < 0.2 denotes forest). The main requirements for SWIR retrievals are (1) SZA < 70° and (2) clear sky conditions. We identify cloud presence every two hours per hemisphere over the two-year period of study (Jan 2015 – Dec 2016). We identify 12 × 12 km (aggregated) cloud free pixels using 3-hour, 0.1° cloud mask data from the International Satellite Cloud Climatology Project (ISCCP) HXG Series dataset (Yong et al., 2018). We re-grid ISCCP data to 0.5° × 0.67° for consistency with MERRA, retaining the number of 0.1° cloud free pixels within each MERRA pixel. We propagate the five scenarios listed in Table S1 as follows: apply Scenarios 1–2 to cold season months (Oct–May), Scenarios 3–4 to early summer (Jun–Jul), and Scenarios 4 and 5 to late summer (Aug–Sep).

AURORA provides extensive sampling of NHL land regions on an annual basis (Figure 1), including summer to fall transition months (August–October, Figure S2), with peak coverage in lower latitudes, and reduced coverage moving north under diminished sunlight and more prevalent temperature inversions. AURORA regional coverage of NHLs exceeds that of OCO-2 by a factor of 100 on a per pixel basis, at the expense of global coverage provided by OCO-2 LEO orbits (Figure S3).

A series of two-year (2015–2016) flux inversion OSSEs are conducted to test the impact of AURORA sampling on CO_2 flux constraints. These OSSEs use the JPL-developed CMS-Flux 4-D variational (4D-Var) inversion system (see Liu et al 2017, 2021) to optimize weekly estimates of net ecosystem exchange (NEE) and ocean fluxes at 4º × 5º spatial resolution. Two OSSEs are conducted, differing in assimilated data: (1) OCO-2 and (2) OCO-2+AURORA. True NEE and ocean fluxes are derived from climatological (2010–2015 mean) posterior fluxes constrained by satellite and surface observations following Byrne et al. (2020). Interannual variations in NEE are added by calculating anomalies in the FLUXCOM 8-day RS NEE dataset scaled by a factor of two to account for the weak interannual variations in this dataset (Jung et al., 2020) Model-based prior fluxes are derived from a suite of 12 dynamic global vegetation models from the TRENDY ensemble (Sitch et al., 2015) version 8 as used in the Global Carbon Budget 2019 (Friedlingstein et al., 2019). We leverage the large ensembles from TRENDY to calculate a prior mean and uncertainty independent of the atmospheric CO_2 data. The uncertainty is inflated by a factor of four to account for the significant bias between prior and true fluxes. We note that this setup creates a realistic situation where the prior uncertainties are specified relative to the actual true–prior flux differences. To test the sensitivity of our results to the prescribed model prior, we provide an additional run using an identical set as described above but replacing the prior flux with output from the CASA biosphere model, which exhibits deeper and earlier summer drawdown compared to TRENDY.

AURORA pseudo-observations (Sec. 2.1.6) are aggregated into super-observations using a 0.5 × 0.625 spatial grid. Following Kulawik et al. (2016), each super-observation is given a measurement error of

$$\left(\frac{(retrieval\ error)^2}{N} + (0.7\ ppm)^2\right)^{1/2}.$$

Retrieval precision is normalized by the square root of the number of cloud-free 4-km pixels within the 0.5° × 0.67° GEOS-Chem grid (denoted *N*). Pseudo XCO_2 data for OCO-2 is extracted from the V10r Level 2 product at GES DISC (10.5067/5Q8JLZL1VD4A). OCO-2 data are averaged into super-observations at 0.5° × 0.5° resolution grids following Liu et al. (2017). Inversion runs are performed from Oct 1, 2014 though Mar 31, 2017. Results are analyzed for the two-year period from 2015–2016, with the first and last three months serving as spin-up/down.

3 Results

We examine the extent to which OCO-2 and AURORA recover the basic seasonal structure (amplitude and timing) of true fluxes, and their anomalies (difference in flux between 2016 and 2015), at different spatial scales ranging from large-, regional-, and grid- scale. For large scale analysis, we integrate posterior fluxes across boreal-arctic (48°–80°N) and midlatitude (28°–48°N) latitude bands, denoted North and South regions, respectively, to assess impacts on the north-south distribution of fluxes and flux anomalies. For regional scale analyses, we aggregate posterior fluxes across discrete regions in Eurasia, characterized by differences in date of temperature zero crossing, to assess detectability of fall emissions is progressively remote and cold climates. Finally, we examine recovery of grid scale fluxes across the pan-Arctic based significant differences in mean signal from zero. We compute grid scale estimate of RMSE based on differences between posterior and true fluxes, then take the difference between the absolute value of the posterior flux and RMSE, denoting flux recovery as significant (denoted below as "detectable"), if the difference is greater than zero. By this definition, neutral fluxes are not detectable.

3.1 Retrieval OSSEs

Single sounding SWIR retrievals show a range of total column DOF (0.5–1.0) and precision (0.45–0.68) depending on the time of year (Figure S4 and Table S2). The highest quality retrievals, characterized by large DOFs and high precision, occur over forested surfaces in summer (DOF = 0.92; Precision = 0.45). In general, the presence of snow and higher SZAs degrade precision and DOF in the SWIR. Aggregating neighboring cloud free pixels into 3 × 3 bins increases DOFs (0.89-1.19) and precision (0.25-0.44).

3.2 Flux Inversion OSSEs

Several key systematic differences between modeled (prior) and expected (truth) flux seasonal amplitude and phase in North (48–80°N) and South (24–48°N) regions provide an important test for satellite-based detection of changing seasonal emissions (e.g., Liu et al., 2022) in northern latitudes. True fluxes exhibit stronger seasonal amplitude and earlier fall onset compared to prior fluxes, and more variable seasonality in the North region (Figure 2).

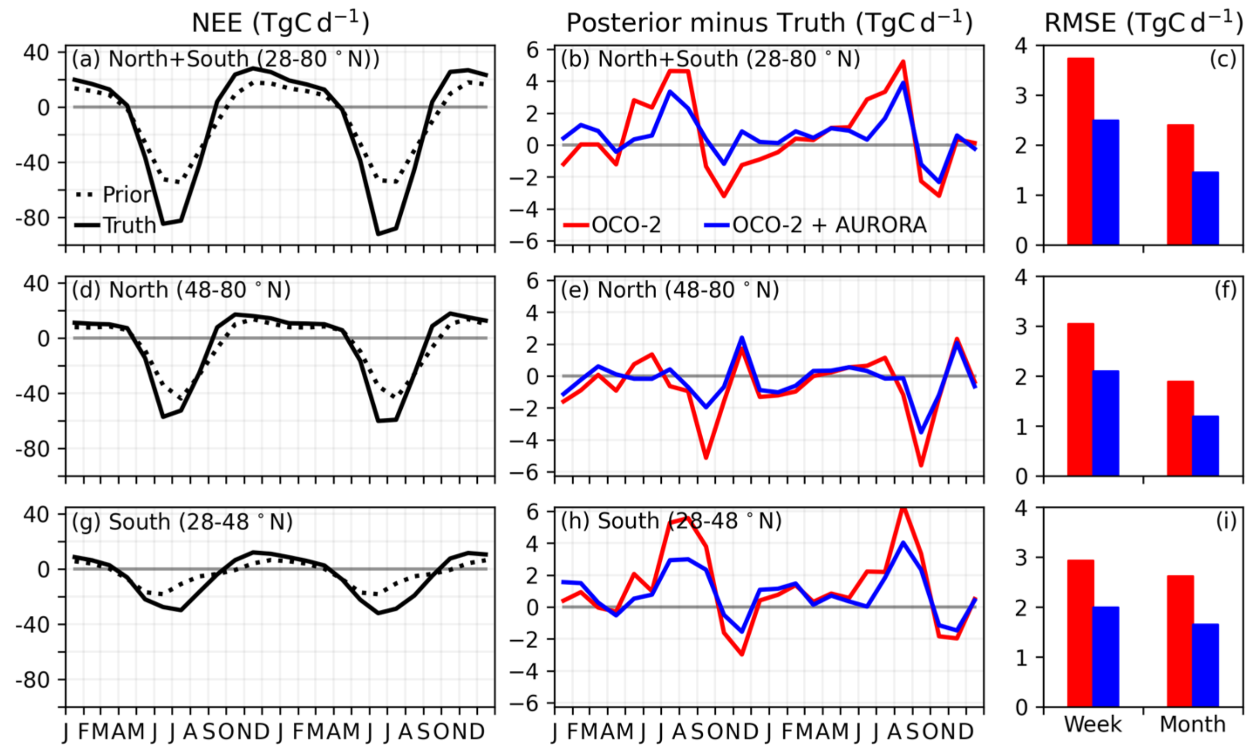

Figure 2: Errors in posterior estimates of seasonal NEE in northern high latitudes (NHL). Aggregated (28–80°N), North (48–80°N), and South (28–48°N) regions are shown from top to bottom, respectively. Prior and True fluxes are shown in the left column posterior (posterior minus true NEE) NEE errors for OCO-2 (red) and OCO-2+AURORA (blue) in the middle column, and weekly- to monthly- mean RMSE in the right column.

OCO-2 recovers a significant portion of the prescribed seasonal structure of true fluxes in south and north NHL regions (Figure S5), with several key exceptions (Figure 2). The first is temporal dipole behavior, characterized by a gradual seasonal swing in the sign of bias in the combined region (28–80°N), from strongly positive in late summer (peaking at ~5 TgC d^{-1}), to weakly negative in fall (peaking at ~2.5 TgC d^{-1}). The presence of temporal dipoles is further indicated in comparisons of annual RMSE values (Figure 2), which are reduced by ~50–100% as temporal aggregation occurs from weekly (3–4 TgC d^{-1}) to monthly (~2 TgC d^{-1}) scales. The second is spatial dipole behavior, indicated by reversed behavior in the sign of the seasonal bias between north and south regions (shift from negative bias in summer to positive bias in fall in the north region). The third is a persistent bias in the timing of the fall zero crossing, characterized by excessive efflux in late summer (before zero crossing) and excessive uptake in the early cold season (after zero crossing).

The addition of AURORA sub-daily sampling diminishes the magnitude and dipole behavior of biases incurred by infrequent OCO-2 sampling. The RMSE is reduced by ~50% on an annual basis, with larger reductions at monthly scale during summer in North and South regions, and during fall in the North region. This significantly improves detection of transitional fluxes and zero crossing date in fall. AURORA has more significant impact during transition and cold season months and exhibits greater return in regions and periods that are poorly observed and/or poorly known.

OCO-2 incurs significant seasonal and meridional dipoles in recovered fluxes (Figures S6). Compensating positive (brown patches) and negative (green patches) biases are present across multiple latitude bands from 30–70°N. NHL posteriors (~60–80°N) shift from positive to negative bias with ~1 month cadence and appear staggered in sign relative to fluxes in adjacent latitudes to the south (~40–60°N). Similar dipole features are seen for OCO-2+AURORA, but with substantially reduced magnitude.

Similar improvements are found in the recovery of seasonal flux anomalies (Figure S7), representing the difference in flux from 2015–2016 when including AURORA compared to OCO-2 alone. Seasonal dipoles persist, but the main features are better captured, and overall variability in the error is reduced throughout the year. For example, OCO-2+AURORA captures most (> 90%) of the negative flux anomaly in the high latitude summer, and a larger fraction of smaller anomalies in spring and early summer. It is noteworthy that AUORA improves detection of dynamic nature of monthly flux anomalies in the South region, compared to more smoothly varying anomalies inferred by OCO-2 alone. Similar improvements are seen at regional scale in Eurasia (Figure S8), with increasingly significant reductions in bias moving eastward and northward from warm (~Europe) to cold (northern Siberia) regions, consistent with increasingly dense and influential coverage from sub-daily sampling These results indicate improved tracking by AURORA of seasonal flux amplitude, timing, and anomalies across latitudes.

Finally, OCO-2+AURORA shows significant improvement in the recovery in the spatial pattern of fall efflux across the pan-Arctic (Figure 3). We define fall efflux as the 30-day period following the NEE zero crossing date when NHL ecosystems transition from net CO_2 sink, when photosynthesis exceeds respiration, to net CO_2 source, when respiration outpaces photosynthesis. OCO-2 flux detectability, representing the percentage of pan-Arctic grid points which are significantly different from zero, is 57%. This increases to 70% with OCO-2+AURORA. The largest improvements occur in Siberia where OCO-2 shoulder season measurements are more limited (67% of Siberian grid cells relative to 34% with OCO-2 alone, assuming Siberia is defined by the domain [90°E-180°E, 45°N-90°N]). The magnitude and spatial pattern of recovered fluxes is also much closer to the truth, as indicated by increased correlation (r = 0.6 *vs.* 0.71) and convergence of slope to the 1:1 line (0.61 *vs*. 0.76) relative to OCO-2 (Figure 3). The recovered fluxes are also better correlated with tree cover in the permafrost region (r = 0.36 *vs*. 0.57), consistent with findings of enhanced fall efflux in high forest Arctic regions (Byrne et al., 2022; Liu et al., 2022).

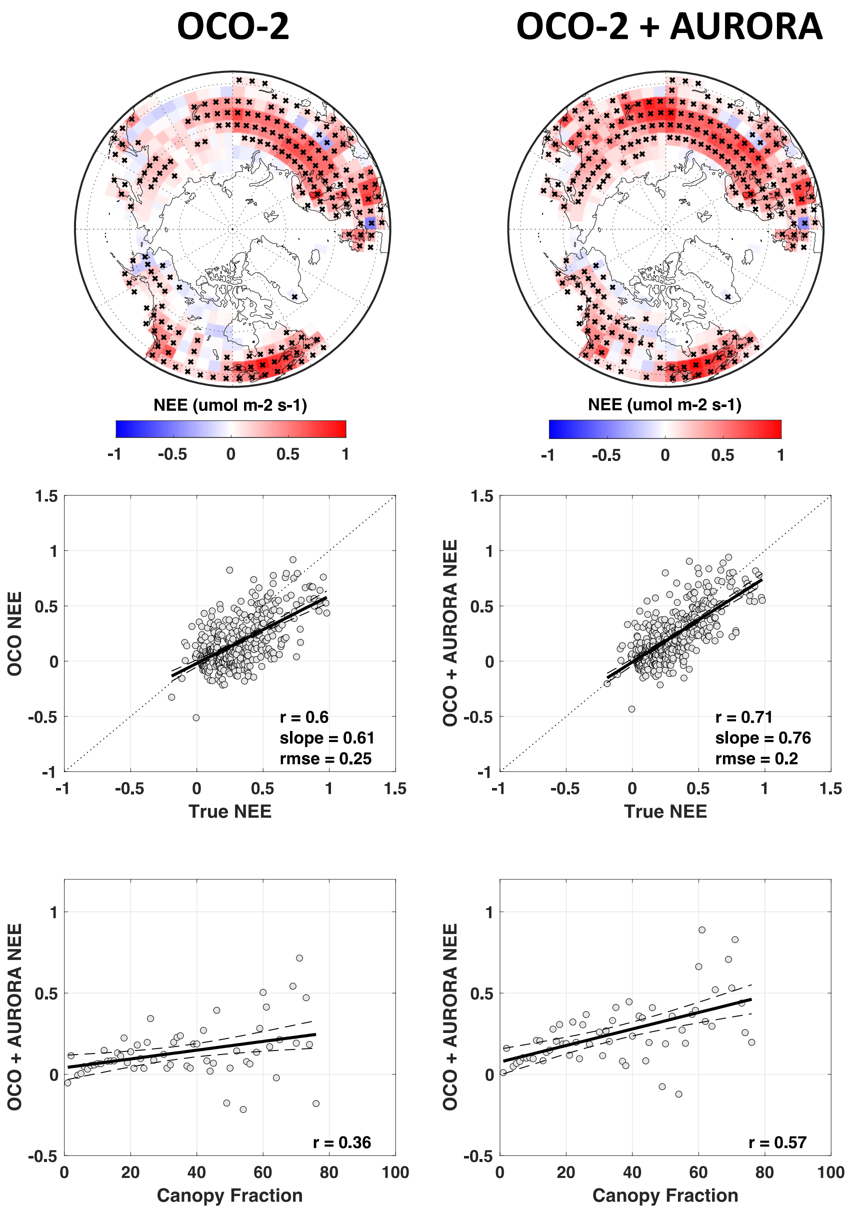

Figure 3: Performance of posterior NEE at grid scale across the pan-Arctic shoulder season. Results for OCO-2 and OCO-2+AURORA are shown in the left and right columns, respectively, and are based on 30-day means for the period of net efflux following fall zero crossing. (top row) Spatial pattern of posterior NEE, where crosses represent "detectable points" that are significantly different from zero, i.e., abs(posterior–truth) > 0. (middle row) Scatter plot of grid-scale posterior vs true NEE shows improvement in slope, correlation, and RMSE when OCO-2 is combined with AURORA. (bottom row) Scatter plot of posterior NEE with canopy fractions shows improved correlation with AURORA, which better captures increasing efflux with increasing forest coverage, consistent with recent findings by Byrne et al. (2022) and Liu et al (2023).

4 Discussion and Conclusions

OCO-2 captures several key features of seasonal CO_2 fluxes in the Arctic. First and foremost, it captures large scale differences in the amplitude and timing of the seasonal cycle in the high (48–80°N) vs middle (28–48°N) latitudes, including deeper and shorter growing season in high latitudes. OCO-2 also captures the jump in CO_2 efflux in early fall, which is prescribed in the true fluxes but missing from the prior, representing a key feature of an accelerating and increasingly labile northern carbon cycle (e.g., Commane et al., 2017; Jeong et al., 2018). Repeated sub-monthly sampling of daylight hours thus provides important constraints on growing and shoulder season fluxes. However, the inability to map concentrations more frequently limits the ability of OCO-2 to accurately place the timing and location of shoulder season fluxes.

Sub-daily mapping of northern high latitudes by AURORA augments flux information from OCO-2 during the critical fall transition period. AURORA's continuous mapping of daytime CO_2 in SWIR bands better resolves spatial gradients of CO_2, which reduces the guesswork required by atmospheric inversion systems in the optimization of surface fluxes to match those gradients, which in turn leads to more accurate seasonal and spatial flux posteriors with smaller errors and reduced dipole features. Our results indicate increased detectability of grid scale and regional fluxes in cold and remote northern Arctic regions, enabled in part by increased daytime sampling of shoulder seasons.

AURORA addresses a key science need that has been identified by the carbon cycle community by providing more frequent measurements of CO_2 efflux during Arctic transition periods. A number of planned missions, including the constellation of LEO satellites from CO2M (and others), are expected to advance upon OCO-2 capabilities with more frequent daytime measurements, providing more accurate pictures of Arctic carbon cycling at regional and potentially grid scale. Planned quasi-geostationary missions such as AOM will provide additional sampling of pan-Arctic transitions seasons, which are expected to further advance grid scale information as demonstrated by AURORA flux inversion OSSEs.

However, the question of what happens during polar twilight and darkness as new carbon in soils, and old carbon in permafrost, is respired back to the atmosphere under increasingly warm fall and winter temperatures is likely to remain a mystery. Addressing this question will require coincident measurements of CO_2 in shortwave and thermal bands, which show significant improvements in the information content (as indicated by the degrees of freedom) in the Arctic (see Text S1) and potential vertical profiling capability, enabling probing closer to the surface, and deeper into the shoulder season, to better localize and extract information. Additional science OSSEs are needed to better characterize thermal retrievals, quantify flux information enabled by combined thermal and shortwave channels, and provide the appropriate science leaps needed to close the Arctic carbon budget.

Acknowledgements

The research was carried out at the Jet Propulsion Laboratory, California Institute of Technology, under a contract with the National Aeronautics and Space Administration (80NM0018D0004). The authors acknowledge support from the Jet Propulsion Laboratory Strategic Research and Technology Development Program.

Open Research

Data Archiving is underway, and has been uploaded as Supporting Information for peer review. Model results will be made available in a public repository (https://cmsflux.jpl.nasa.gov/) upon publication.

References

Bruhwiler, L., Parmentier, F.J.W., Crill, P., Leonard, M. and Palmer, P.I., 2021. The Arctic carbon cycle and its response to changing climate. *Current Climate Change Reports*, *7*, pp.14-34.

Byrne, B., Liu, J., Lee, M., Baker, I.,Bowman, K. W., Deutscher, N. M., et al.(2020). Improved constraints on northern extratropical CO_2 fluxes obtained by combining surface-based and space-based atmospheric CO_2 measurements. Journal of Geophysical Research: Atmospheres, 125, e2019JD032029. https://doi.org/10.1029/2019JD032029.

Byrne, B., Liu, J., Yi, Y., Chatterjee, A., Basu, S., Cheng, R., Doughty, R., Chevallier, F., Bowman, K.W., Parazoo, N.C. and Crisp, D., 2022. Multi-year observations reveal a larger than expected autumn respiration signal across northeast Eurasia. *Biogeosciences*, *19*(19), pp.4779-4799.

Commane, R., Lindaas, J., Benmergui, J., Luus, K.A., Chang, R.Y.W., Daube, B.C., Euskirchen, E.S., Henderson, J.M., Karion, A., Miller, J.B. and Miller, S.M., 2017. Carbon dioxide sources from Alaska driven by increasing early winter respiration from Arctic tundra. *Proceedings of the National Academy of Sciences*, *114*(21), pp.5361-5366.

Friedlingstein, P., O'sullivan, M., Jones, M.W., Andrew, R.M., Hauck, J., Olsen, A., Peters, G.P., Peters, W., Pongratz, J., Sitch, S. and Le Quéré, C., 2020. Global carbon budget 2020. *Earth System Science Data Discussions*, *2020*, pp.1-3.

Jeong, S. J., Bloom, A. A., Schimel, D., Sweeney, et al. (2018). Accelerating rates of arctic carbon cycling revealed by long-term atmospheric CO_2 measurements. *Science Advances*, *4*(7), 1–7.

Jung, M., Schwalm, C., Migliavacca, M., Walther, S., Camps-Valls, G., Koirala, S., et al. (2020). Scaling carbon fluxes from eddy covariance sites to globe: synthesis and evaluation of the FLUXCOM approach. Biogeosciences,17 (5), 1343–1365. 0.

Kulawik, S. S., Osterman, G., Jones, D. B. A., and Bowman, K. W.: Calculation of altitude-dependent Tikhonov constraints for TES nadir retrievals, IEEE T. Geosci. Remote, 44, 1334–1342, https://doi.org/10.1109/TGRS.2006.871206, 2006.

Kulawik, S., Wunch, D., O'Dell, C., Frankenberg, C., Reuter, M., Oda, T., Chevallier, F., Sherlock, V., Buchwitz, M., Osterman, G., Miller, C. E., Wennberg, P. O., Griffith, D., Morino, I., Dubey, M. K., Deutscher, N. M., Notholt, J., Hase, F., Warneke, T., Sussmann, R., Robinson, J., Strong, K., Schneider, M., De Mazière, M., Shiomi, K., Feist, D. G., Iraci, L. T., and Wolf, J.: Consistent evaluation of ACOS-GOSAT, BESD-SCIAMACHY, CarbonTracker, and MACC through comparisons to TCCON, Atmos. Meas. Tech., 9, 683–709, https://doi.org/10.5194/amt-9-683-2016, 2016.

Liu, J., Bowman, K.W., Schimel, D.S., Parazoo, N.C., Jiang, Z., Lee, M., Bloom, A.A., Wunch, D., Frankenberg, C., Sun, Y. and O'Dell, C.W., 2017. Contrasting carbon cycle responses of the tropical continents to the 2015–2016 El Niño. *Science*, *358*(6360), p.eaam5690.

Liu, Z., Kimball, J.S., Ballantyne, A.P., Parazoo, N.C., Wang, W.J., Bastos, A., Madani, N., Natali, S.M., Watts, J.D., Rogers, B.M. and Ciais, P., 2022. Respiratory loss during late-growing season determines the net carbon dioxide sink in northern permafrost regions. *Nature Communications*, *13*(1), p.5626.

Nassar et al. (2014), CO_2 from HEO …, Journal of Geophysical Research, https://agupubs.onlinelibrary.wiley.com/doi/full/10.1002/2013JD020337

Nassar et al. (2019), AIM-North, Canadian Journal of Remote Sensing https://www.tandfonline.com/doi/full/10.1080/07038992.2019.1643707

Nassar, R., MacDonald, C.G., Kuwahara, B., Fogal, A., Issa, J., Girmenia, A., Khan, S. and Sioris, C.E., Intelligent Pointing increases the fraction of cloud-free CO2 and CH4 observations from space. *Frontiers in Remote Sensing*, *4*, p.1233803. https://www.frontiersin.org/articles/10.3389/frsen.2023.1233803/full

Natraj, V., Luo, M., Blavier, J.-F., Payne, V. H., Posselt, D. J., Sander, S. P., Zeng, Z.-C., Neu, J. L., Tremblay, D., Wu, L., Roman, J. A., Wu, Y.-H., and Dorsky, L. I.: Simulated multispectral temperature and atmospheric composition retrievals for the JPL GEO-IR Sounder, Atmos. Meas. Tech., 15, 1251–1267, https://doi.org/10.5194/amt-15-1251-2022, 2022.

Natraj, V., R. J. D. Spurr, A. Guo, T. Le, Z.-C. Zeng, S. Fan, and Y. L. Yung (2023), The 2 Stream-Exact Single Scattering (2S-ESS) Radiative Transfer Model, J. Quant. Spectrosc. Radiat. Transfer, 295, 108416, doi:10.1016/j.jqsrt.2022.108416.

Natali, S.M., Watts, J.D., Rogers, B.M., Potter, S., Ludwig, S.M., Selbmann, A.K., Sullivan, P.F., Abbott, B.W., Arndt, K.A., Birch, L. and Björkman, M.P., 2019. Large loss of CO2 in winter observed across the northern permafrost region. *Nature Climate Change*, *9*(11), pp.852-857.

Parazoo, N. C., Commane, R., Wofsy, et al (2016). Detecting regional patterns of changing CO_2 flux in Alaska. *PNAS*, *113*(28).

Rantanen, M., Karpechko, A.Y., Lipponen, A., Nordling, K., Hyvärinen, O., Ruosteenoja, K., Vihma, T. and Laaksonen, A., 2022. The Arctic has warmed nearly four times faster than the globe since 1979. *Communications Earth & Environment*, *3*(1), p.168

Schiferl, L.D., Watts, J.D., Larson, E.J., Arndt, K.A., Biraud, S.C., Euskirchen, E.S., Goodrich, J.P., Henderson, J.M., Kalhori, A., McKain, K. and Mountain, M.E., 2022. Using atmospheric observations to quantify annual biogenic carbon dioxide fluxes on the Alaska North Slope. *Biogeosciences*, *19*(24), pp.5953-5972.

Sitch, S., Friedlingstein, P., Gruber, N., Jones, S.D., Murray-Tortarolo, G., Ahlström, A., Doney, S.C., Graven, H., Heinze, C., Huntingford, C. and Levis, S., 2015. Recent trends and drivers of regional sources and sinks of carbon dioxide. *Biogeosciences*, *12*(3), pp.653-679.

Spurr, R., and Natraj, V.: A linearized two-stream radiative transfer code for fast approximation of multiple-scatter fields, J. Quant. Spectrosc. Ra., 112, 2630–2637, https://doi.org/10.1016/j.jqsrt.2011.06.014, 2011.

Watts, J.D., Farina, M., Kimball, J.S., Schiferl, L.D., Liu, Z., Arndt, K.A., Zona, D., Ballantyne, A., Euskirchen, E.S., Parmentier, F.J.W. and Helbig, M., 2023. Carbon uptake in Eurasian boreal forests dominates the high-latitude net ecosystem carbon budget. *Global Change Biology*, *29*(7), pp.1870-1889.

Xi, X., Natraj, V., Shia, R. L., Luo, M., Zhang, Q., Newman, S., Sander, S. P., and Yung, Y. L.: Simulated retrievals for the remote sensing of CO_2, CH_4, CO, and H_2O from geostationary orbit, Atmos. Meas. Tech., 8, 4817–4830, https://doi.org/10.5194/amt-8-4817-2015, 2015.

Zeng, Z.-C., Natraj, V., Xu, F., Pongetti, T. J., Shia, R.-L., Kort, E. A., Toon, G. C., Sander, S. P., and Yung, Y. L.: Constraining aerosol vertical profile in the boundary layer using hyperspectral measurements of oxygen absorption, Geophys. Res. Lett., 45(19), 10772–10780, https://doi.org/10.1029/2018gl079286, 2018.

Zeng, Z.-C., Zhang, Q., Natraj, V., Margolis, J. S., Shia, R.-L., Newman, S., Fu, D., Pongetti, T. J., Wong, K. W., Sander, S. P., Wennberg, P. O., and Yung, Y. L.: Aerosol scattering effects on water vapor retrievals over the Los Angeles Basin, Atmos. Chem. Phys., 17(4), 2495–2508, https://doi.org/10.5194/acp-17-2495-2017, 2017.

Zhang, Q., Natraj, V., Li, K.-F., Shia, R.-L., Fu, D., Pongetti, T. J., Sander, S. P., Roehl, C. M., and Yung, Y. L.: Accounting for aerosol scattering in the CLARS retrieval of column averaged CO_2 mixing ratios, J. Geophys. Res., 120(14), 7205–7218, https://doi.org/10.1002/2015jd023499, 2015.

Zhang, Q., Shia, R.-L., Sander, S. P., and Yung, Y. L.: XCO_2 retrieval error over deserts near critical surface albedo, Earth Space Sci., 3(2), 36–45, https://doi.org/10.1002/2015ea000143, 201